ResearchGate

See discussions, stats, and author profiles for this publication at: https://www.researchgate.net/publication/13647348

Determination of the three-dimensional solution structure of Raphanus sativus Antifungal Protein 1 by 1H NMR1

ARTICLE *in* JOURNAL OF MOLECULAR BIOLOGY · JUNE 1998

Impact Factor: 4.33 · DOI: 10.1006/jmbi.1998.1767 · Source: PubMed

CITATIONS
112

READS
55

4 AUTHORS, INCLUDING:

Wim Vranken
Vrije Universiteit Brussel
71 PUBLICATIONS **3,117** CITATIONS
SEE PROFILE

Willem Broekaert
University of Leuven
126 PUBLICATIONS **12,356** CITATIONS
SEE PROFILE

Available from: Wim Vranken
Retrieved on: 24 January 2016

J. Mol. Biol. (1998) **279**, 257–270

JMB

Determination of the Three-dimensional Solution Structure of *Raphanus sativus* Antifungal Protein 1 by ^{1}H NMR

Franky Fant[1], Wim Vranken[1], Willem Broekaert[2] and Frans Borremans[1]*

[1]*Biomolecular NMR Unit, Department of Organic Chemistry, University of Gent Belgium*

[2]*F.A. Janssens Laboratory of Genetics, Department of Applied Plant Sciences Katholieke Universiteit, Leuven Belgium*

**Corresponding author*

Raphanus sativus Antifungal Protein 1 (Rs-AFP1) is a 51 amino acid residue plant defensin isolated from radish (*Raphanus sativus* L.) seeds. The three-dimensional structure in aqueous solution has been determined from two-dimensional ^{1}H NMR data recorded at 500 MHz using the DIANA/REDAC calculation protocols. Experimental constraints consisted of 787 interproton distances extracted from NOE cross-peaks, 89 torsional constraints from 106 vicinal interproton coupling constants and 32 stereospecific assignments of prochiral protons. Further refinement by simulated annealing resulted in a set of 20 structures having pairwise root-mean-square differences of 1.35(±0.35) Å over the backbone heavy atoms and 2.11(±0.46) Å over all heavy atoms. The molecule adopts a compact globular fold comprising an α-helix from Asn18 till Leu28 and a triple-stranded β-sheet (β1 = Lys2-Arg6, β2 = His33-Tyr38 and β3 = His43-Pro50). The central strand of this β-sheet is connected by two disulfide bridges (Cys21–Cys45 and Cys25–Cys47) to the α-helix. The connection between β-strand 2 and 3 is formed by a type VIa β-turn. Even the loop (Pro7 to Asn17) between β-strand 1 and the α-helix is relatively well defined. The structure of *Raphanus sativus* Antifungal Protein 1 features all the characteristics of the ''cysteine stabilized αβ motif''. A comparison of the complete structure and of the regions important for interaction with the fungal receptor according to a mutational study, is made with the structure of γ-thionin, a plant defensin that has no antifungal activity. It is concluded that this interaction is both electrostatic and specific, and some possible scenarios for the mode of action are given.

© 1998 Academic Press Limited

Keywords: plant defensin; γ-thionin; cysteine-stabilized αβ motif; simulated annealing; protein structure

Introduction

Plant defensins are a class of cysteine-rich peptides which are typically 45 to 54 amino acids long (51 for Rs-AFP1; Figure 1), have a net positive charge and contain eight cysteine residues that are involved in four disulfide bridges (Broekaert *et al.*, 1995). These plant defensins have been devided in three groups according to their biological activity (Broekaert *et al.*, 1995). The members of the first two groups inhibit growth of a broad range of fungi. They have in general no or little activity against bacteria and cause no adverse effects on cultured human cells (Terras *et al.*, 1992). Members of the first group of antifungal plant defensins cause reduced elongation of fungal hyphae with an increase in hyphal branching (Terras *et al.*, 1992). The plant defensins from the Brassicaceae (including *Raphanus sativus* Antifungal Protein 1,

Abbreviations used: DQF-COSY, two-dimensional double-quantum filtered correlation spectroscopy; E.COSY, exclusive two-dimensional correlation spectroscopy; FID, free induction decay; JR-NOESY, jump and return two-dimensional nuclear Overhauser enhancement spectroscopy; NOESY, two-dimensional nuclear Overhauser enhancement spectroscopy; Rs-AFP1, *Raphanus sativus* Antifungal Protein 1; TOCSY, two-dimensional total correlation spectroscopy; TPPI, time proportional phase incrementation; pGlu, pyroglutamic acid.

0022–2836/98/210257–14 $25.00/0/mb981767

© 1998 Academic Press Limited

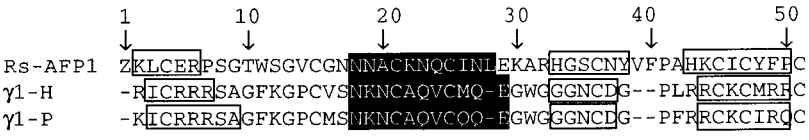

Figure 1. Amino acid sequence of Rs-AFP1, γ1-H thionin and γ1-P thionin. Z is the one letter code for pyroglutamic acid. The disulphide bridges (not shown) are Cys4–Cys51, Cys15–Cys36, Cys21–Cys45 and Cys25–Cys47. The α-helical region is indicated by a black bar and the β-strands by a box.

Rs-AFP1) and the Saxifragaceae belong to this group (Terras *et al*., 1992, 1993; Osborn *et al*., 1995). On the other hand, the plant defensins from the Asteraceae, the Fabaceae and the Hippocastanaceae slow down fungal growth but do not cause morphological distortions (Osborn *et al*., 1995). The antifungal activity of the members of these two groups of plant defensins is reduced by the presence of cations, with divalent cations being at least one order of magnitude more potent than monovalent cations (Terras *et al*., 1992, 1993; Osborn *et al*., 1995). This antagonistic effect is strongly dependent on the fungus and hence does not originate from a conformational change of the protein but from an interaction between fungi and cations (Terras *et al*., 1992; Osborn *et al*., 1995).

The plant defensins of the third group show no antifungal activity *in vitro* but instead inhibit α-amylases (Bloch & Richardson, 1991) and the protein synthesis in cell-free systems (Colilla *et al*., 1990; Mendez *et al*., 1990). This group contains the γ-thionins from wheat and barley (Colilla *et al*., 1990; Mendez *et al*., 1990), ω-hordothionin (García *et al*., 1993) and SIα from *Sorghum bicolor* (Bloch & Richardson, 1991). In contrast, no α-amylase inhibitory activity was detected for any of the members of the two first groups (Osborn *et al*., 1995).

The *Raphanus sativus* species was chosen as a model plant to study the role of antifungal plant defensins in host defense (Terras *et al*., 1995). By immunocytochemistry, it was shown that Rs-AFP1 is stored in the middle lamellae of the cell walls of different radish seed tissues, where it may play a role in the protection of the seeds against seed-borne or soil-borne fungal diseases. Indeed, Rs-AFP1 was shown to be preferentially released from germinating radish seeds in amounts sufficient to create a zone around the seeds in which fungal growth is suppressed. In addition, Rs-AFP1 homologs are synthesized *de novo* in radish leaves in response to fungal attack (Terras *et al*., 1995), where they may contribute to an induced defense mechanism. Overexpression of an Rs-AFP1 homolog in transgenic tobacco plants resulted in enhanced resistance to the fungal pathogen *Alternaria longipes* (Terras *et al*., 1995).

In contrast to insect and mammalian defensins (Cociancich *et al*., 1993; Cornet *et al*., 1995; Kagan *et al*., 1990), antifungal plant defensins do not cause ion channel formation, in either artificial planar lipid bilayers or artificial liposomes. However, when added to fungi they cause an increase in Ca^{2+} influx and K^+ efflux, and an increase of the pH of the medium (Thevissen *et al*., 1996). The effects on the membrane potential are somewhat different for the two groups of antifungal plant defensins. Plant defensins from the first group cause hyperpolarization of the fungal membrane in contrast to the depolarization caused by the members of the second group (Thevissen *et al*., 1996). The growth inhibition of the fungal hyphae caused by antifungal plant defensins, is supposedly the result of increased Ca^{2+} influx, which destroys the concentration gradient of cytosolic Ca^{2+}. These cytosolic Ca^{2+} gradients are essential for driving polarized growth in fungal hyphae (Jackson & Heath, 1993; Garrill *et al*., 1993).

The sequence specific assignment of the proton resonances and the secondary structure of the radish antifungal plant defensin Rs-AFP1 have been reported previously (Fant *et al*., 1997). Here, we present the solution structure of Rs-AFP1 determined by ^{1}H NMR. It is shown that Rs-AFP1 has a compact three-dimensional structure and possesses all the characteristics of the cysteine stabilized αβ motif. This is a common motif found in some scorpion toxins (Kobayashi *et al*., 1991) and insect defensins (Cornet *et al*., 1995). Based on the determined structure, some insight is gained into the event of recognition between Rs-AFP1 and its putative target site on fungal hyphae, and some possible modes of action are postulated.

Results

Distance calculation and stereospecific assignments

The build-up of NOE intensity with mixing time was monitored for typical NOE-contacts. At 160 ms the build-up is still close to linear. Thus, at this mixing time the isolated spin pair approximation is valid and contribution of spin diffusion to the NOE cross-peak can be neglected. A total of 775 NOEs from the NOESY spectrum in H_2O and ^2H_2O were converted to distance constraints with the program CALIBA. Their classification (intraresidual, sequential, medium-range and long-range contacts) and distribution over the sequence is shown in Figure 2a. Torsion angle constraints were obtained from 44 $^3J_{N\alpha}$ and 62 $^3J_{\alpha\beta}$ coupling constants. The $^3J_{N\alpha}$ coupling constants were calculated from the separation of cross-peak extrema measured in two transforms (one phased in absorption and the other in pure dispersion) of the DQF-COSY spectrum (Kim & Prestegard, 1989).

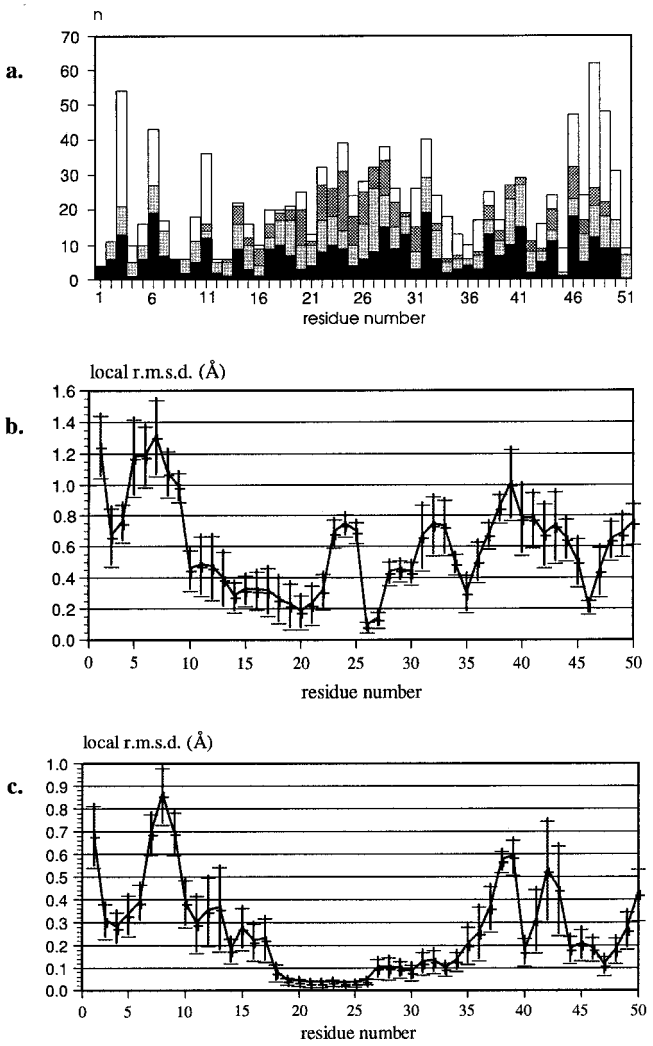

Figure 2. Plot (a) of the number n of NOE distance constraints d_{ij} per residue, *versus* the amino acid sequence of Rs-AFP1. The NOE contacts are specified as: intraresidual (in total 373), filled black; sequential (in total 156), filled grey; medium-range ($|i-j| \leqslant 5$; in total 101), cross-hatched; and long-range ($|i-j| > 5$; in total 145), open. Also the local r.m.s.d. values for the 20 simulated annealing structures of Rs-AFP1 for all the atoms (b) and for the backbone atoms (c) are given. A residue is assigned its local r.m.s.d. value by superimposing a tripeptide fragment of which it is the central amino acid.

The $^3J_{\alpha\beta}$ coupling constants were derived from an E.COSY spectrum (Griesinger *et al.*, 1985, 1987).

Stereospecific assignments were obtained with HABAS (Güntert *et al.*, 1989) for 18 prochiral β-methylene groups: Lys2, Leu3, Cys4, Ser8, Trp11, Cys15, Asn18, Cys21, Asn23, Cys25, Asn27, Leu28, Glu29, His33, Asn37, Tyr38, Cys47 and Phe49. Comparison of the experimental $^3J_{\alpha\beta}$ coupling constants with the theoretical autocorrelation diagram for $^3J_{\alpha\beta2}$ and $^3J_{\alpha\beta3}$ (Nagayama & Wüthrich, 1981) showed that of the 18 residues with stereospecific assignments for the C^β protons, Leu3, Cys4, Trp11, Cys15, Cys21, Cys25, Asn27, Tyr38, Cys47 and Phe49 have a side-chain which is conformationally rigid with respect to the dihedral angle χ^1. Only these stereospecific assignments were retained and completed with the manual assignments (Kline *et al.*, 1988; Zuiderweg *et al.*, 1985) of the β-methylene group of Pro41 and the β-methyl groups of Val14. The 89 generated intervals for the dihedral angles ϕ, ψ and χ^1 were modified according to the criteria given by Kördel *et al.* (1993).

Structure calculation and refinement

The distance constraints were multiplied with a factor of 1.1 in order to obtain upper limits and to account for experimental errors. The disulphide bridges between Cys4–Cys51, Cys15–Cys36, Cys21–Cys45 and Cys25–Cys47 were implemented by means of upper and lower limits for the distances between the S^γ atoms and between the C^β and S^γ atom of both cysteine residues (Williamson *et al.*, 1985). In the same way the N-terminal pyroglutamine ring of Rs-AFP1 (Terras *et al.*, 1992) was closed.

Of the 500 generated DIANA structures, 50 had a target function between 0.77 and 2.65 Å^2. The values of ϕ, ψ and χ^1 for the central residue of each tripeptide segment, with conformations that are in agreement with the experimental and the van der Waals constraints, were determined. By comparing these dihedral angle intervals with the intervals generated by HABAS (Widmer *et al.*, 1989) additional stereospecific assignments were obtained for the β-methylene group of Lys30 and Phe40, both residues having a rigid side-chain. From the 25 best structures 18 additional stereospecific assignments (αCH_2 of Gly13 and Gly34; βCH_2 of Glu29, Cys36, His43, Tyr48 and Cys51; γCH_2 of Glu29, Pro41, Ile46; δCH_2 of Pro41 and Pro50; δCH_3 of Leu28; δNH_2 of Asn17, Asn18, Asn23 and Asn27; and εNH_2 of Gln24) were obtained with the program GLOMSA (Güntert *et al.*, 1991). The same 25 structures were used to define six hydrogen bonds in agreement with the exchange rates (Table 1; Fant *et al.*, 1997). These hydrogen bonds were enforced by upper and lower limits.

With these additional data the best 43 structures of the 500 generated by DIANA, have final target functions between 1.03 and 2.00 Å^2. Based on the first distinct jump in the value of the target function and on an analysis of the violations, the first 25 structures were taken as being representative of the ensemble of conformations that are in agreement with the experimental data (Table 2). The maximum pairwise standard deviation *versus* the target function value for the first 50 structures was used as a criterium to verify that this small set of structures is still representative of the conformation of the protein (Widmer *et al.*, 1993).

These 25 structures were used as starting structures for simulated annealing using the AMBER forcefield (Weiner *et al.*, 1984). The constraints that define the disulphide bonds and the N-terminal pyroglutamine ring were removed from the exper-

Table 1. Hydrogen bonds and slowly exchanging amide protons in Rs-AFP1

Acceptor	Donor	Number[a]	k_m (10^{-2} min^{-1})[b]
Lys2 O	Lys2 $H^{\xi 2}$	13	>20
Leu3 O	Lys2 $H^{\xi 3}$	11	>20
Cys51 O	Lys2 $H^{\xi 1}$	14	>20
Phe49 O	Cys4 NH	20	>20
Cys4 O	Phe49 NH	20	0.26
Cys47 O	Arg6 NH	20[c]	0.84
Arg6 O	Cys47 NH	20	0.98
Ser8 O	Arg6 H^{η}	10	>20
Thr10 $O^{\gamma 1}$	Trp11 NH	15	>20
Thr10 O	Ser12 NH	14	Overlap
Thr10 O	Ser12 H^{γ}	11	>20
Val14 O	Trp11 $H^{\varepsilon 1}$	20	>20
Trp11 O	Gly13 NH	15	>20
His43 O	Cys15 NH	17	0.82
Cys15 O	Asn17 NH	18	Overlap
Asn17 $O^{\delta 1}$	Ala20 NH	20	>20
Asn17 O	Cys21 NH	20	Overlap
Asn18 $O^{\delta 1}$	Lys22 $H^{\varepsilon 2}$	18	>20
Asn18 $N^{\delta 2}$	Cys36 NH	12	3.87
Ser35 O^{γ}	Asn18 $H^{\delta 21}$	17	>20
Cys36 O	Asn18 $H^{\delta 21}$	10	>20
Asn18 O	Lys22 NH	20[c]	Overlap
Asn19 O	Asn23 NH	20	Overlap
Ala20 O	Gln24 NH	20[c]	0.63
Cys21 O	Cys25 NH	20[c]	Overlap
Lys22 O	Ile26 NH	20[c]	0.83
Asn23 $O^{\delta 1}$	Asn27 $H^{\delta 21}$	20	>20
Asn23 O	Asn27 NH	20	1.56
Gln24 O	Leu28 NH	20	>20
Cys25 O	Glu29 NH	20[c]	1.20
Ile26 O	Lys30 $H^{\varepsilon 3}$	18	>20
Asn27 O	Lys30 $H^{\varepsilon 2}$	18	>20
Leu28 O	Lys30 $H^{\varepsilon 1}$	16	>20
Lys30 O	Arg32 $H^{\eta 11}$	12	>20
Tyr48 O	Arg32 NH	17	4.20
His33 O	Tyr48 NH	20	0.44
Ile46 O	Ser35 NH	20	Overlap
Ser35 O	Ile46 NH	16	0.98
Lys44 O	Asn37 NH	14	>20
Asn37 O	Lys44 NH	17	>20
Pro41 O	Tyr38 H^{η}	17	>20
Phe40 O	Lys44 $H^{\varepsilon 1}$	20	>20
Ala42 O	Lys44 $H^{\varepsilon 2}$	14	>20

[a] This column lists how many of the 25 simulated annealing structures reveal the corresponding hydrogen bond according to the criteria $d_{DA} \leqslant 2.8$ Å and $\theta_{DHA} > 155°$.

[b] Rate constant for NH/N^2H exchange at 305.3 K and pH 4.2 (Fant *et al.*, 1997).

[c] For these hydrogen bonds distance constraints were implemented in the structure calculation.

imental data, since these are implemented as covalent bonds in AMBER. At this stage three and nine additional distance constraints were extracted from, respectively, a ''jump and return''-NOE-spectrum ($\tau_m = 160$) and NOESY spectra with a shorter mixing time. The amide bonds were kept planar by additional torsional constraints (Skelton *et al.*, 1995). In Rs-AFP1, only Pro41 possesses a *cis* peptide bond (Fant *et al.*, 1997). From the 25 calculated structures, five were rejected on the basis of local distortion (Kördel *et al.*, 1993), thus leaving 20 structures for further analysis. From Table 2 it is clear that the total energy drops without increasing violations on the experimental constraints.

Table 2. Target functions, no. of constraints, residual violations on the constraints, energies and r.m.s.d. values for the 25 best DIANA structures and the 20 best structures after simulated annealing (with the AMBER forcefield) for Rs-AFP1.

Parameter	DIANA	DIANA-SA
Target function (Å^2)	1.35 ± 0.13	
No. of distance constraints (upper/lower)		
NOE	775/0	787/0
Hydrogen bond	12/12	12/12
S–S bond	12/12	0/0
Ring closure of pyroglutamine	1/1	0/0
No. of torsional constraints	89	139
Upper limit violations		
Number > 0.2 Å	0.88 ± 0.88	0.05 ± 0.22
Number > 0.1 Å	6.24 ± 2.11	1.85 ± 1.39
Sum of violations (Å)	2.43 ± 0.47	1.94 ± 0.20
Maximum violation (Å)	0.28 ± 0.15	0.13 ± 0.04
Lower limit violations		
Number > 0.2 Å	0.16 ± 0.37	0.00 ± 0.00
Number > 0.1 Å	1.08 ± 0.76	0.00 ± 0.00
Sum of violations (Å)	0.27 ± 0.10	0.01 ± 0.01
Maximum violation (Å)	0.14 ± 0.06	0.01 ± 0.01
Dihedral angle violations		
Number > 5°	0.04 ± 0.20	0.10 ± 0.31
Sum of violations (°)	3.77 ± 2.39	28.22 ± 5.72
Maximum violation (°)	1.59 ± 1.25	3.93 ± 0.97
Total AMBER energy (kcal mol^{-1})	2124.26 ± 77.09	−716.24 ± 12.35
r.m.s.d. value (Å)		
Backbone atoms (N, C^{α}, C′, O)	1.20 ± 0.25	1.35 ± 0.35
Heavy atoms	2.12 ± 0.33	2.11 ± 0.46

The complete structure calculation cycle was repeated three times. Only the results of the third cycle are given here. The first cycle contained only the unambiguously assigned NOE contacts (689 in total). Based on the resulting simulated annealing structures, the remaining ambiguous NOE cross-peaks were assigned. The contact was used if only one combination of all possible connection partners corresponded to a distance shorter than 5 Å in all 25 structures. The second cycle started with 759 NOE cross-peaks. Only in the third cycle were hydrogen bond constraints included. As more constraints were used per cycle the lowest target function for the structures in each cycle increased (0.66, 1.10 and 1.03 Å^2 for the first, second and third cycle, respectively) and the r.m.s.d. value for the backbone atoms decreased (1.95(±0.25) Å, 1.74(± 0.21) Å and 1.35(±0.35) Å for the first, second and third cycle, respectively).

Description of the structure

The distribution in the Ramachandran plot of all the residues of the best 20 structures obtained by simulated annealing (Figure 3) indicates the overall quality: 71.1% of the residues are in most favoured regions, 25.7% in additional allowed regions, 1.8% in generously allowed regions and 1.4% in disallowed regions (definitions according to Laskowski *et al.*, 1993). The residues in the generously allowed

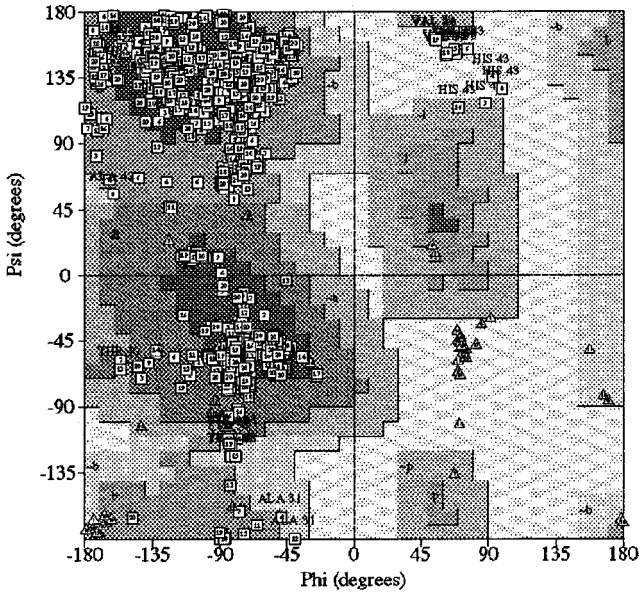

Figure 3. Ramachandran plot for all residues of the 20 best simulated annealing structures of Rs-AFP1. The most favoured [A,B,L] (71.1% of the residues), additional allowed [a,b,l,p] (25.7%), generously allowed [~ a, ~ b, ~ l, ~ p] (1.8%) and disallowed regions (1.4%) are represented in different grey-values. The proline residues (Pro7, Pro41 and Pro50) and the end residues (Glu1 and Cys51) are not shown, the glycine residues are indicated by triangles. This Figure was generated by PROCHECK (Laskowski *et al.*, 1993).

and disallowed regions are mainly situated in the less well defined loop between β-strand 1 and the α-helix (*vide supra* and Fant *et al.*, 1997) as can be concluded from Figure 2b and c and the Ramachandran plots per residue of the 20 structures (not shown). The RMS Z-scores for bond lengths, bond angles and impropers are, respectively, 0.666, 1.081 and 0.948.

Rs-AFP1 adopts a compact globular fold (Figure 4a) comprising an α-helix from Asn18 till Leu28 and a triple-stranded β-sheet (β1 = Lys2 to Arg6, β2 = His33 to Tyr38 and β3 = His43 to Pro50). The central strand of this β-sheet is connected by two disulfide bridges (Cys21–Cys45 and Cys25–Cys47) to the α-helix (Figure 4b).

The α-helix extends 16.3 Å and is spanning 11 residues from Asn18 till Leu28 (three helical turns), which is evidenced by an abrupt change in ϕ and ψ dihedral angles with respect to the residues preceding Asn18 and following Leu28. The values of the dihedral angles for the Asn18–Leu28 fragment are within 20° of the regular α-helix values of −57° and −48°. Only the ϕ and ψ angles of Ile26 and the ϕ angle of Asn27 have characteristic values for a 3_{10} helix ($\phi = -74°$ and $\psi = -4°$). The close proximity (2.6 Å) of the carbonyl groups of Glu29 and Ile26 may be at the origin of the deviation of the carbonyl group orientation of Ile26 from the normally expected quasi-parallel orientation with respect to the α-helix axis (Figure 5). The ϕ,ψ values of Glu29 reflect this local distortion of the α-helix. Glu29 adopts a polyproline conformation which has been frequently observed in short con-

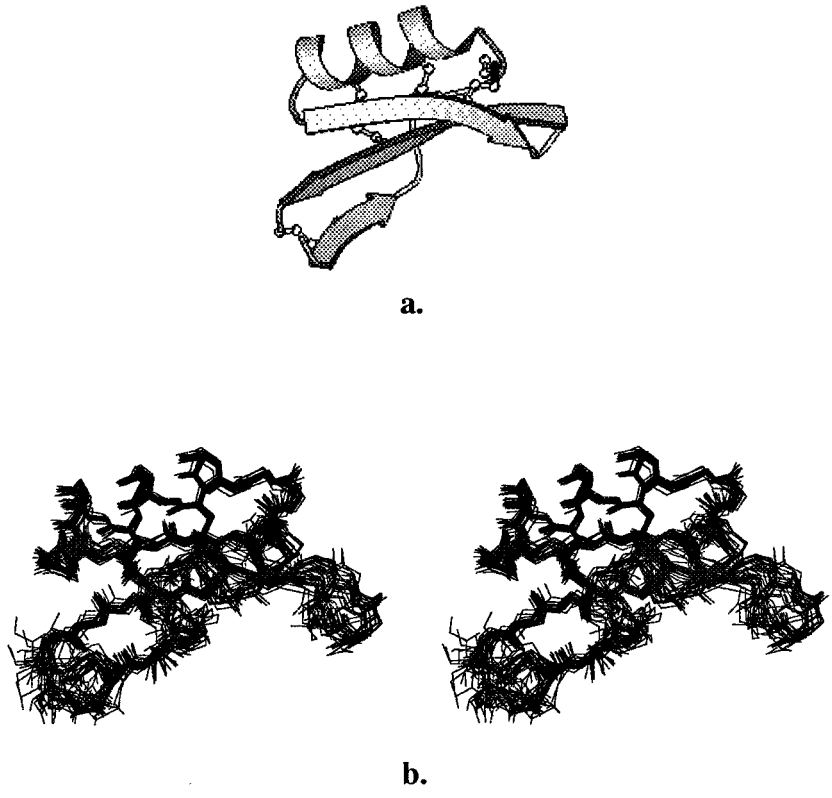

Figure 4. Schematic MOLSCRIPT (Kraulis, 1991) representation (a) of the main secondary structure elements of Rs-AFP1 and stereoview (b) of the polypeptide backbone and the disulphide bridges in the 20 best simulated annealing structures of Rs-AFP1. All the structures were superimposed on the first structure to give a maximal overlap.

nections between α and β secondary structure elements (Richardson & Richardson, 1989). From Figures 4b and 5 it can be seen that the α-helix is defined with high precision (see also very low local r.m.s.d. values in Figure 2b and c). In the α-helix region, the expected typical pattern of NH_i–CO_{i+4} hydrogen bonds and the slow amide NH/N^2H exchange (except for Leu28) are indeed

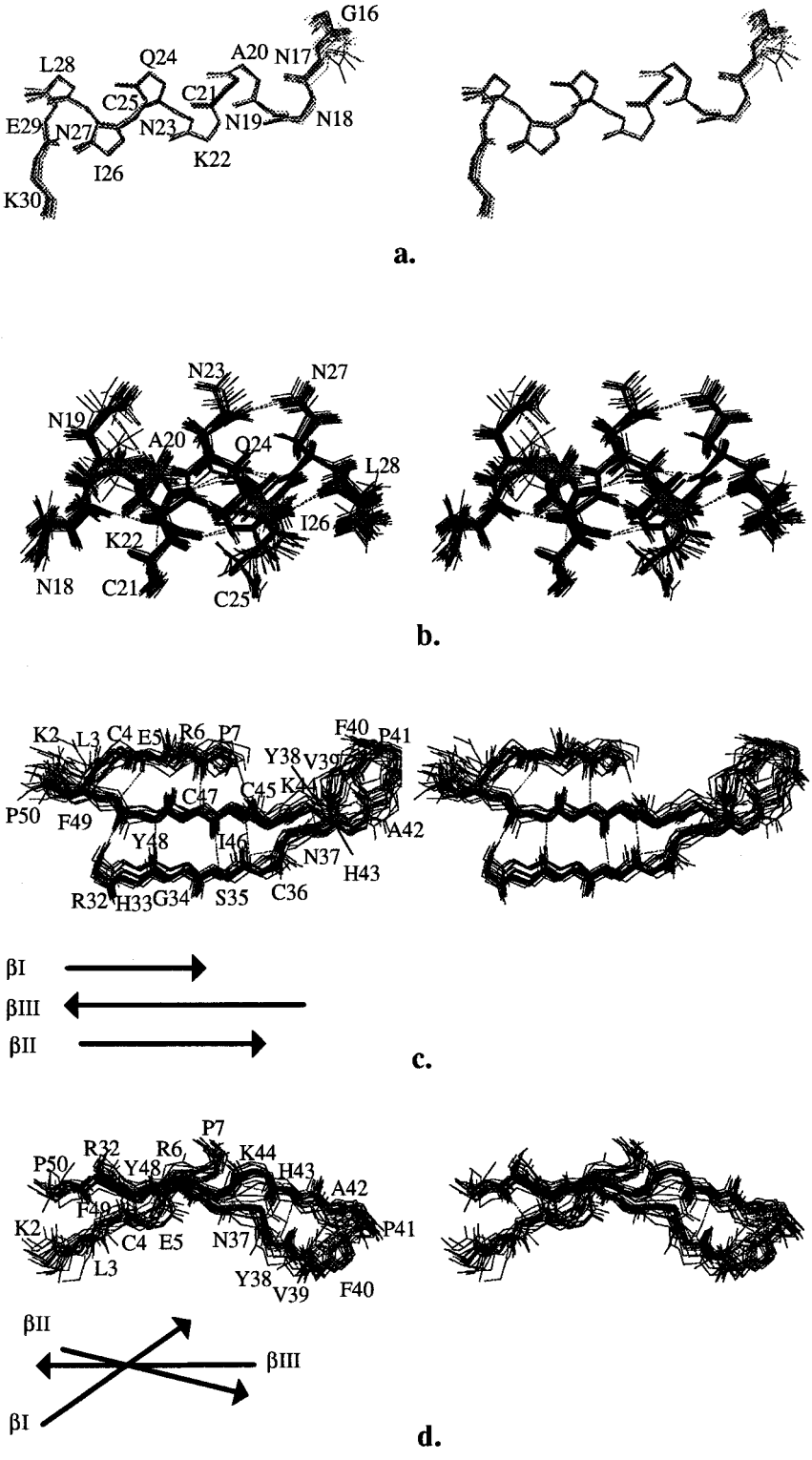

Figure 5. Stereoview of the Rs-AFP1 backbone without (a,c,d) and with side-chains (b) for selected parts of the molecule: the α-helix with the flanking residues (a), the α-helix (b), the anti-parallel triple-stranded β-sheet in top view (c), and in side view (d).

observed (Table 1). Due to the tensioactive behaviour of Rs-AFP1, the rates for the amide protons that exchange moderately slowly could not be determined (Fant *et al*., 1997). In all 20 simulated annealing structures the criteria that define a hydrogen bond (distance between donor and acceptor atom <2.8 Å, and angle between donor, hydrogen and acceptor atom >155°) are fulfilled for the backbone and side-chain carbonyl of Asn17 with the amide protons of, respectively, Cys21 and Ala20. The backbone of Asn17 has a β-conformation, which is often observed for an N-capping asparagine (Richardson & Richardson, 1989). The last four backbone carbonyl groups of the α-helix (Cys25, Ile26, Asn27 and Leu28) can form a hydrogen bond with, respectively, the amide proton of Glu29 and the three protons of the $N^{\varepsilon}H_3^+$ group of the Lys30 side-chain, thus resulting in so called C-capping (Richardson & Richardson, 1989). The helix is further stabilized by a hydrogen bond between the side-chain carbonyl group of Asn23 and a side-chain amide proton of Asn27.

The α-helix is connected by two disulphide bridges (Cys21–Cys45 and Cys25–Cys47) to the central strand (β-strand 3) of an antiparallel β-sheet (β1:Lys2 to Arg6, β2:His33 to Tyr38 and β3:His43 to Pro50). The higher r.m.s.d. values of the backbone for each β-strand (0.69(±0.19) Å, 0.56(±0.16) Å and 0.63(±0.14) Å for, respectively, β1, β2 and β3) as compared to the value for the α-helix (0.18(±0.05) Å) indicate their less precise definition The anti-parallel orientation is evidenced by the nine hydrogen bonds geometrically recognized. For all amide protons involved in these hydrogen bonds slow NH/N^2H exchange was observed with the exception of Cys4, Asn37 and Lys44 (Table 1). β-Strand 2 shows a kink around Cys36 and β-strand 1 makes an angle of 25° with β-strand 3 and an angle of 40° with β-strand 2. This is the result of the right-handed twist of β-strand 1 (and to a lesser extent of β-strand 2) around β-strand 3. The axis of the α-helix and β-strand 2 are not oriented parallel but cross at an angle of 30°. The intersection of the α-helix and β-strand 2 occurs at, respectively, Lys22 and Gly34, leaving no space for a side-chain at position 34. This has been already observed for small scorpion toxins and used to explain the highly conserved appearance of glycine at this position among the proteins with the same motif (Bontems *et al*., 1992).

The connection between β-strands 2 and 3 is made by a type VI β-turn featuring a *cis* proline in position $i+2$. The ϕ, ψ angles for the two central residues $i+1$ and $i+2$ (−60°, 120° and −90°, −50°) resemble those of the type VIa (−60°, 120° and −90°, 0°) more than those of the type VIb (−120°, 120° and −60°, 150°; Yao *et al*., 1994). Although Yao *et al*. (1994) showed that the stability of this kind of turn is mainly originating from hydrophobic contacts, the type VI β-turn in Rs-AFP1 seems to be also stabilized by hydrogen bonds between the side-chain amine protons of Lys44 and the carbonyl groups of Phe40 and Ala38, and between the side-chain hydroxyl group of Tyr38 and the carbonyl group of Pro41. Although this β-turn is protruding into and exposed to the solvent, its backbone r.m.s.d. value of 0.39(±0.21) Å is small.

The turn between the α-helix and β-strand 2 is made up by five residues, Glu29, Lys30, Ala31, Arg32 and His33 (which has a β-conformation and also belongs to β-strand 2), and adopts a βγβαβ-conformation (notation according to Efimov, 1986). Thus the turn is composed of two half turns (βγβ and βαβ), each making a 90° change in direction. A combination of two half turns in α/β-structures is very often observed, since a classical turn (180°) brings the interconnected secondary structure elements close to each other (Efimov, 1993). The very low backbone r.m.s.d. value of 0.20(±0.07) Å (comparable to the one of the helix) indicates that this turn is defined with high precision.

The loop between β-strand 1 and the α-helix, the fragment Pro7 to Asn17, has a relatively high backbone r.m.s.d. value of 1.24(±0.26) Å, which originates mainly from the relatively poorly defined first part of the loop (Pro7 to Gly9). The loop itself is composed of eight half turns with backbone atoms forming two perpendicular planes (plane 1: Pro7 to Thr10; plane 2: Ser12 to Asn17 and Trp11

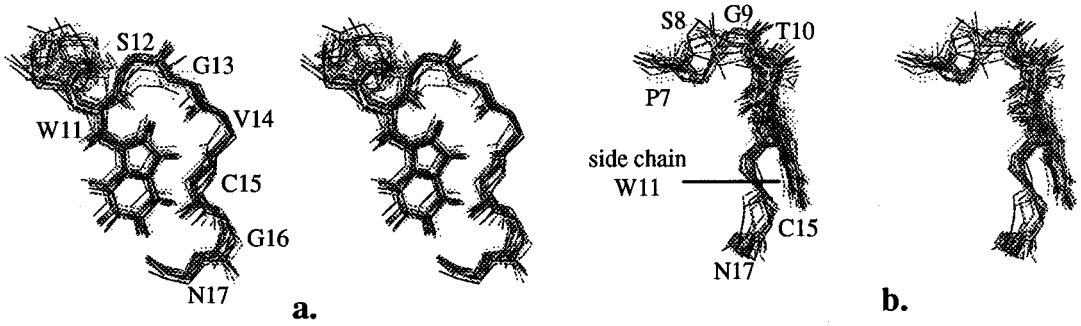

Figure 6. Stereoview of the polypeptide backbone of the Pro7 to Asn17 fragment and the side-chain of Trp11 in two different orientations: parallel with (a) and perpendicular to (b) the indole ring.

in the centre; Figure 6). The second plane coincides with the plane of the indole ring of Trp11 (Figure 6a). Segment Pro7 to Trp11 (Figure 6b) contains the half turns Pro7-Ser8-Gly9 (α/β-β/α-α/α_L), Ser8-Gly9-Thr10 (β/α-α/α_L-α) and Gly9-Thr10-Trp11 (α/α_L-α-β) and is connected by the fourth half turn Thr10-Trp11-Ser12 ($\alpha\beta\delta$) to the second plane (Figure 6b), which contains the half turns Trp11-Ser12-Gly13 ($\beta\delta\varepsilon$), Gly13-Val14-Cys15 ($\varepsilon\beta\alpha$), Val14-Cys15-Gly16 ($\beta\alpha\alpha_L$) and Cys15-Gly16-Asn17 ($\alpha\alpha_L\beta$). Due to the ambiguous conformations of the first three turns in the poorly defined segment Pro7 to Trp11, only three hydrogen bonds can be recognized on the basis of geometric parameters, i.e. between the backbone carbonyl groups and the backbone amide protons of, respectively, Thr10 and Ser12, Trp11 and Gly13, and Cys15 and Asn17. The tryptophan residue appears to be crucial for the stabilization of this loop. Indeed, the polypeptide chain wraps around the indole ring (Figure 6) and the $N^{\varepsilon 1}$ proton of Trp11 can form a hydrogen bond with the carbonyl group of Val14.

The three-dimensional structure of Rs-AFP1 is dictated in part by the four disulphide bonds. Cys21 and Cys25 are on the same side of the helix and easily form two disulphide bonds with the two cysteine residues located at the same side of β-strand 3 (Cys45 and Cys47). These two disulphide bonds as well as the disulphide bond between Cys15 and Cys36, which connects the loop and β-strand 2, adopt a left-handed spiral conformation. The fourth disulphide bond, Cys4–Cys51, holds the N and C termini together and adopts a rather unusual right-handed hook (Richardson & Richardson, 1989).

Evaluation of the convergence of the side-chains shows a correlation with the classification of rigid and flexible side-chains according to the autocorrelation diagram for $^3J_{\alpha\beta 2}$ and $^3J_{\alpha\beta 3}$ (*vide supra*). This is not surprising, since for all rigid residues a stereospecific assignment of the prochiral β-methylene groups was found (and retained), thus avoiding the use of pseudo-atom corrections. A correlation between the convergence and the solvent accessibility of the residue was not observed. But almost all residues with a rigid side-chain are hydrophobic or are cysteine. Exceptions are Asn17, Asn27 and Lys30 whose side-chains are involved in hydrogen bonds (Table 1). For the same reason, the side-chains of Asn18 and Asn23 are well defined although they were assigned as flexible. Leu28 and Phe40 are the only hydrophobic residues with a flexible side-chain. Both belong to the group of residues important for interaction with fungi (*vide infra*). Leu28 was assigned as flexible and Phe40 as rigid; this poor convergence of Phe40 can be a result of the protruding of the type VI β-turn and the resulting lack of constraints. Remarkable is the fact that one of the key residues for the antifungal activity, Lys44, has the less well defined side-chain.

Rs-AFP1 has an ellipsoid-like molecular shape with a length of 35 Å and a basis of 25 Å on 30 Å. The most solvent accessible residues, as calculated with the program PROCHECK (Laskowski *et al*., 1993), are located in the type VIa β-turn and at the N and C termini and, to a lesser extent, in the loop between β-strand 1 and the helix, and in the turn between the helix and β-strand 2.

Discussion

Structural relationships with other proteins

The structure of Rs-AFP1 features all the characteristics of the ''cysteine stabilized α-helix motif''. This motif was first recognized by Kobayashi *et al*. (1991). They observed that the structures of a series of small neurotoxins isolated from venoms of scorpions and honey bees feature an α-helical fragment (Cys-Xaa-Xaa-Xaa-Cys) connected by two disulphide bonds to a β-strand (Cys-Xaa-Cys). Cornet *et al*. (1995) later proposed the term ''cysteine stabilized αβ motif'' (CSαβ) for this particular fold. According to the definition by Cornet *et al*. (1995), these structures are further stabilized by at least a third disulphide bond given the following consensus sequence: Cys^{I}-$(Xaa)_i$-Cys^{II}-Xaa-Xaa-Xaa-Cys^{III}-$(Xaa)_j$-Gly-Xaa-$Cys^{I'}$-$(Xaa)_k$-$Cys^{II'}$-Xaa-$Cys^{III'}$ (in Rs-AFP1 is I = 15, II = 21, III = 25, I′ = 36, II′ = 45 and III′ = 47). Rs-AFP1 is a βαββ protein according to the general definition of Orengo & Thornton (1993). Hitherto there are three groups of βαββ proteins known to adopt the CSαβ motif. The short-chain scorpion toxins including, charybdotoxin (Bontems *et al*., 1992), iberiotoxin (Johnson & Sugg, 1992), kaliotoxin (Fernández *et al*., 1994), margatoxin (Johnson *et al*., 1994), agitoxin 2 (Krezel *et al*., 1995) and noxiustoxin (Dauplais *et al*., 1995) all belong to the first group of proteins that are 36 to 39 amino acids long, contain three disulphide bonds and act on Ca^{2+}-activated K^+ channels.

The second group comprises the long-chain scorpion toxins, including ''Old World-like'' neurotoxin (Jablonsky *et al*., 1995), ''variant-1'' neurotoxin (Lee *et al*., 1994) and ''variant-3'' neurotoxin (Zhao *et al*., 1992), all three from the scorpion *Centruroides sculpturatus*; potent toxin II (Fontecilla-Camps *et al*., 1988), toxine III (Mikou *et al*., 1992) and the anti-insect toxin (Darbon *et al*., 1991) of the scorpion *Androctonus australis*; Cll toxin 1 of the scorpion *Centruroides limpidus* (Lebreton *et al*., 1994); and anti-insect toxin III of the scorpion *Leiurus quinquestriatus* (Landon *et al*., 1996). They are all 60 to 70 amino acids long, contain four disulphide bonds and inhibit Na^+ channels.

Chlorotoxin, which is isolated from the venom of the scorpion *Leiurus quinquestriatus* is 36 amino acids long, contains four disulphide bonds and blocks Cl^- channels. It has therefore the characteristics of the short-chain and the long-chain toxins (Lippens *et al*., 1995).

The third group contains the plant defensins γ1-H thionin and γ1-P thionin (Bruix *et al*., 1993), ω-hordothionin (Bruix *et al*., 1995) and Rs-AFP1. The γ-thionins are 91% mutually homologous but

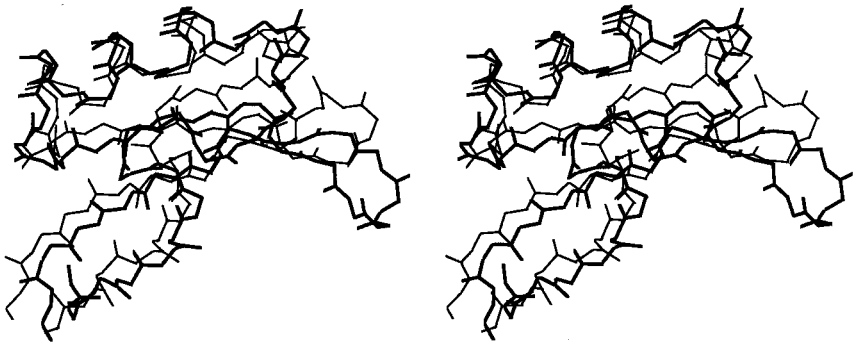

Figure 7. Superposition of the backbone atoms of the helix and the β-strands of Rs-AFP1 (thick line) and γ1-P thionin (thin line).

only 53% homologous to Rs-AFP1. Although these three proteins contain the same elements of secondary structure (Figure 1) and the same global fold (Figure 7) they have a different activity and specificity. Rs-AFP1 is a potent inhibitor of fungal growth (Terras *et al*., 1992) whereas γ1-H and γ1-P are devoid of substantial antifungal activity but are inhibitors of protein synthesis in cell-free systems (Collila *et al*., 1990; Mendez *et al*., 1990; Osborn *et al*., 1995). These three structures differ mainly in the conformation of the loop between β-strand 1 and the α-helix, and in the loop between β-strand 2 and β-strand 3. This is reflected by a relatively high value for the standard deviation of the backbone atoms (6.70 Å and 6.65 Å) between the best structure of Rs-AFP1 and γ1-H and γ1-P thionin, respectively. This value drops if only the backbone atoms of the helix and the β-strands are superimposed (1.88 and 1.81 Å, respectively). The structures of both thionins are very similar (standard deviation of 1.00 Å). In Rs-AFP1, the loop between β-strand 1 and the α-helix is one residue longer, but the meaning of this difference is difficult to interpret as this loop is poorly defined in all three proteins (Bruix *et al*., 1993). Only Rs-AFP1 features the type VI β-turn with a *cis* proline, which sticks more outwards because the flanking β-strands 2 and 3 both are one residue longer. The more protuberant β-turn of Rs-AFP1 results from the increased number of residues between $Cys^{I'}$ and $Cys^{II'}$ (eight residues between Cys36 and Cys45) as compared to the γ-thionins (six residues between Cys34 and Cys41).

In short-chain scorpion toxins the number of residues between these two cysteine residues is correlated with a difference in activity and specificity (Krezel *et al*., 1995). This region seems to be involved in the interaction with a receptor (Krezel *et al*., 1995; Dauplais *et al*., 1995). A similar correlation between the length of the corresponding loop in long-chain scorpion toxins and their specific activity has been recognized by Fontecilla-Camps *et al*. (1988) from comparison of the structures of the variant-3 toxin of *Centruroides sculpturatus* Ewing (Zhao *et al*., 1992) and other toxins from *Androctonus australis* Hector (Fontecilla-Camps *et al*., 1988).

Structure-activity relationship

De Samblanx *et al*. (1997) have performed a mutational analysis of Rs-AFP2, an isoform of Rs-AFP1 that differs from Rs-AFP1 by only two residues. In that study, different amino acid residues were substituted by their corresponding residues of SIα2, a plant defensin that is devoid of antifungal activity and resembles closely γ1-P thionin and γ1-H thionin. In addition, some variants were produced in which particular residues were replaced by the basic amino acid arginine. Amino acid residues that had a significant effect on the antifungal activity of substitution variants were located in either of two subsites comprising: (i) residues in the protruding domain consisting of the type VIa β-turn and the first part of β-strand 3 (e.g. Tyr38, Phe40, Pro41, Ala42, Lys44 and Ile46), and (ii) residues in the loop connecting β-strand 1 and the α-helix and contiguous residues on the α-helix and the last part of β-strand 3 (e.g. Thr10, Ser12, Leu28 and Phe49). Both subsites are adjoining and form an elongated patch along one side of the molecule (De Samblanx *et al*., 1997). Interestingly, the β-turn region and the loop between β-strand 1 and the α-helix, which appear to be key structural elements for the interaction with the fungal target site according to the mutational analysis, are the regions in which the structure of Rs-AFP1 deviates most strongly from those of the inactive plant defensins γ1-P thionin and γ1-H thionin (*vide supra*).

The mutational analysis has also revealed that basic amino acid residues contribute to the antifungal potency of Rs-AFP2. Replacement of Lys44 by a neutral glutamine reduced the antifungal potency, while substitution of the neutral residues Gly9 and Val39 by arginine increased the antifungal potency (De Samblanx *et al*., 1997).

The electrostatic potential surface of Rs-AFP1 as calculated with the program MOLMOL (Koradi *et al*., 1996) shows that positive charges at the surface, together with the negative charge originating

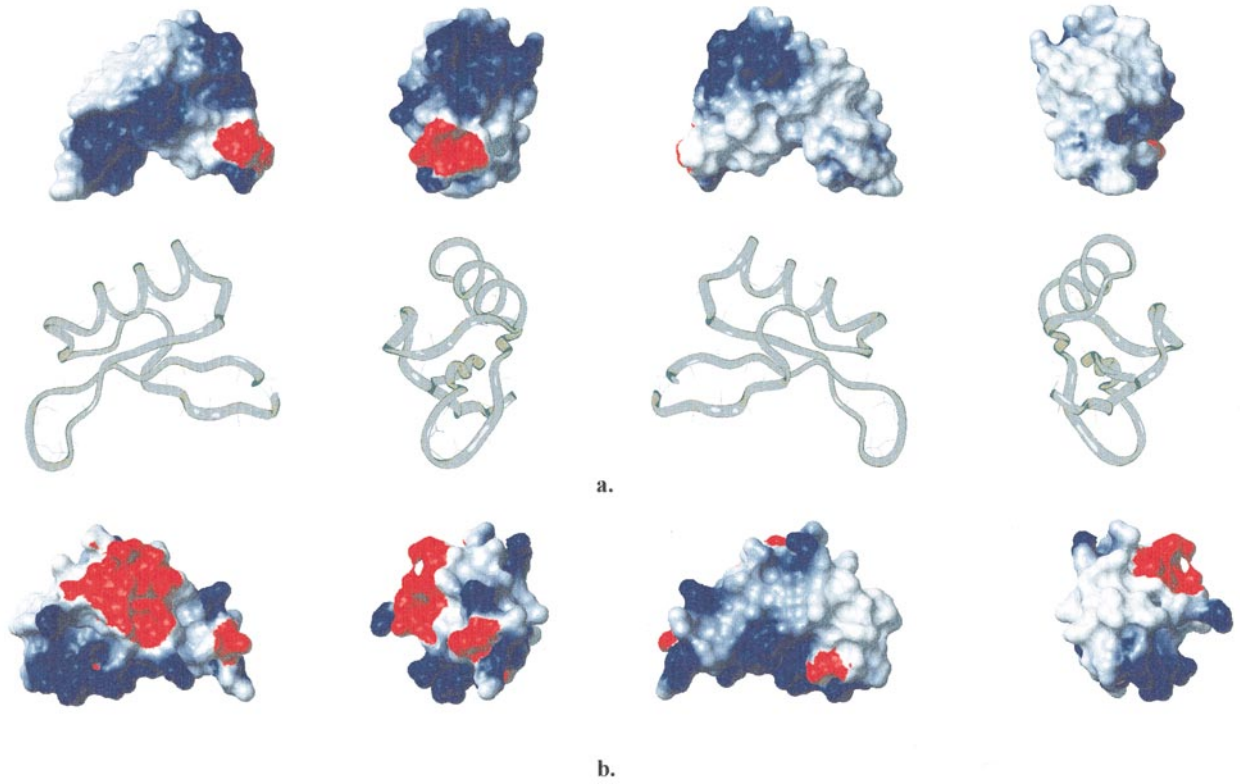

Figure 8. Electrostatic potential surface calculated with MOLMOL (Koradi *et al.*, 1996) of Rs-AFP1 (a) and γ1-P thionin (b) in four different orientations obtained by rotation of 90° around the vertical axis. The corresponding ribbon presentation is also given for Rs-AFP1. The positive and negative charges are coloured, respectively, in blue and red.

from Glu5, are mainly located at one side of the molecule (Figure 8a). This lining of positive charges forms half a torus around the molecule. The charge distribution is completely different in the γ-thionines (Figure 8b). The positive charges are alternated with negative charges which are randomly distributed over the molecule.

These patches of positive charges of Rs-AFP1 correspond to the subsites that had been identified to be important for antifungal activity based on the mutational analysis. At the type VI β-turn, only the concave side of the turn is postively charged. Hence, it is expected that the interaction between Rs-AFP1 and its fungal target site is based in part on electrostatic interactions. It should also be noted that the more basic Rs-AFP2 variant in which Val39 had been replaced by arginine was more active than wild-type Rs-AFP2 against the fungi *Fusarium culmorum*, *Nectria haematococca* and *Verticillium dahlia*, all belonging to the Pyrenomycetes, but less active against *Phomabetae*, belonging to the Loculoascomycetes (De Samblanx *et al.*, 1997). This indicates that specificity must exist between antifungal plant defensins and their fungal target site.

Previous studies on the mode of action of plant defensins have indicated that they cause a rapid Ca^{2+} influx and K^{+} efflux across fungal membranes (Thevissen *et al.*, 1996). As plant defensins do not alter the electrical properties of artificial phospholipid membranes, it is assumed that the ion fluxes are not the result of direct interactions between phospholipids and the plant defensins, but rather from indirect events initiated by specific recognition between plant defensins and a membrane receptor. Further support to this assumption comes from our observation that intact fungal hyphae and plasma membrane microsomes derived from fungal hyphae contain high affinity binding sites for Hs-AFP1, an antifungal plant defensin from *Heuchera sanguinea* which exerts similar morphogenic effects on fungi as Rs-AFP1 (Thevissen *et al.*, 1997). Addition of excess Rs-AFP2 reduced binding of radiolabelled Hs-AFP1, indicating that both proteins compete for the same binding sites. Interestingly, a single amino acid substitution variant of Rs-AFP2, in which the Tyr38 was replaced by glycine, was unable to compete for the Hs-AFP1 binding sites (Thevissen *et al.*, 1997). The same Rs-AFP2 variant had previously been shown to be virtually devoid of antifungal activity and to be unable to induce ion fluxes in fungal hyphae, thus suggesting a causal link between receptor binding and ion flux induction. Different scenarios, all speculative as yet, can be envisaged to explain these events. First, it is possible that the receptor itself is an ion channel that is activated upon binding of the plant defensin ligand. An argument in favour of this hypothesis is that Rs-AFP1 is structurally related to different types of scorpion toxins that are known to interact with either Ca^{2+}, Na^{+} or Cl^{-} channels (Bontems *et al.*, 1992; Krezel *et al.*, 1995; Jablonsky *et al.*, 1995;

Lippens *et al*., 1995; Landon *et al*., 1996). However, in all these cases the ion channel is blocked rather than activated. On the other hand, an example of an ion channel that is activated upon recognition by a peptide ligand has recently been described (Zimmerman *et al*., 1997). Parsley cells contain a particular Ca^{2+} channel that opens upon binding of a peptide derived from a fungal cell wall glycoprotein. This channel is considered to be the first component in a signal transduction pathway that is used by parsley cells to activate defense-related genes upon detection of a fungal pathogen. The signal transduction events involve in this case Ca^{2+} influx, K^+ efflux and alkalinisation of the external medium (Nürnberger *et al*., 1994), which bears a strong similarity with the events observed in the interaction between plant defensins and fungi (Thevissen *et al*., 1996). A second scenario to explain the plant defensin-fungus interaction assumes the existence of a membrane receptor that acts as an anchor point allowing the plant defensin to slip into the membrane. This would then result in ion channel formation, either by the plant defensin itself or in conjuction with the receptor. An example of this type of interaction is that between the pore-forming killer toxin K1 and a high-affinity binding site residing on the plasma membrane of *Saccharomyces cerevisiae*, which facilitates insertion of killer toxin K1 in the plasma membrane (Schmitt & Compain, 1995). A third possibility, finally, is that binding of plant defensins to a membrane receptor triggers the activation of a series of ion channels *via* secondary messengers. Discrimination between these different models will require the identification of the binding partner of plant defensins on fungal hyphae. Once such a receptor is identified, the interaction with plant defensins can be studied in depth and knowledge of the precise three-dimensional structure of Rs-AFP1 and of the residues involved in exerting antifungal activity will form a valuable structural basis for these types of studies.

Materials and Methods

NMR measurements

Rs-AFP1 was isolated and purified according to a described procedure (Terras *et al*., 1992) and dissolved in 0.5 ml of either 9:1 (v/v) $H_2O/^2H_2O$ or in ^2H_2O to give a final protein concentration of 1.3 mM. At higher concentrations the assignment of the resonances is hampered by severe broadening and overlap of lines, presumably as a result of intermolecular association. Spectra were recorded on a Bruker AM-500 spectrometer at 305.3 K and pH 4.2 (without any correction for the isotope effect). Chemical shifts are quoted relative to internal sodium 2,2-dimethyl-2-silapentane-5-sulphonate (DSS).

The DQF-COSY (Rance *et al*., 1983; Neuhaus *et al*., 1985) and the NOESY spectrum with mixing times 70, 100, 130, 160, 200 and 250 ms (Kumar *et al*., 1980) and with a spectral width of 6493.51 Hz, were recorded with TPPI (Marion & Wüthrich, 1983). The water signal was suppressed by presaturation during the one second relaxation delay and during the mixing time in the NOESY experiments (Wider *et al*., 1983) except for the JR-NOESY (mixing time 160 ms and ''jump and return'' delay 170 μs). For the DQF-COSY 700 FIDs of size 2048, 192 scans each were recorded, preceded by four dummy scans. The NOESY spectra were obtained with typically 512 t_1 experiments (160 scans and four dummy scans per experiment) and 2048 real data points each. Prior to Fourier transformation, all the data matrices were multiplied by a $\pi/4$ shifted squared sine window function in the t_2 dimension and a $\pi/3$ shifted sine window function in the t_1 dimension. The digital resolution in both dimensions was 3.17 Hz/pt. Residual baseline distortions were removed with a fifth-order polynomial. The NOESY spectra were manually integrated in PRONTO with baseline correction and in median-mode.

Accurate values for the $^3J_{\alpha\beta}$ coupling constants were derived from an E.COSY spectrum (Griesinger *et al*., 1985, 1987) in ^2H_2O with a spectral width of 5263 Hz. 1024 FIDs of size 4096 and 192 scans each, were recorded. The same data processing was used (*vide supra*). A strip transformation of the data resulted in a final resolution of 0.32 Hz/pt in F_2 and 0.64 Hz/pt in F_1. $^3J_{N\alpha}$ coupling constants and amide proton exchange rates were determined as reported previously (Fant *et al*., 1997).

Structure calculations

Two different calibration curves describing the relationships between the NOESY cross-peak volumes and the corresponding distances were used with the program CALIBA (Güntert *et al*., 1991) for the non-methyl and the methyl containing contacts. The different classes of cross-peaks were individually calibrated based on characteristic distances. Upper limits on the distance constraints were 1.1 times the calculated distances and no lower limits based on these distances were used.

All structure calculations were performed with the program DIANA version 2.1 (Güntert *et al*., 1991) using the REDAC protocol (Güntert & Wüthrich, 1991). Pseudoatom corrections were added as described by Güntert *et al*. (1991). The number of iterations in each minimalisation step was 1200 and 1800 for, respectively, the heavy and all atoms. Each step was halted if the target function changed by less than 1% after 800 iterations.

The 25 structures with lowest target function were subjected to simulated annealing in the AMBER forcefield (Weiner *et al*., 1984). All distance constraints and dihedral angle constraints were enforced through the usual harmonic ''pseudo'' energy-term with force constants of 32 kcal mol^{-1} $Å^{-2}$ (Moore *et al*., 1991) and 100 kcal mol^{-1} rad^{-2}, respectively. A distance-dependent dielectric constant was used. During the complete simulated annealing the weighting coefficients were 1.0 except for the chirality constraint, which was 10.0. The structures were first energy minimized by 150 iterations by steepest descent and 500 iterations by conjugate gradients followed by heating of the molecule to 1000 K in 2 ps and kept at this temperature during 18 ps. The time steps were always 1 fs. The molecule was then cooled to 300 K in eight steps (850 K, 750 K, 675 K, 600 K, 525 K, 425 K and 375 K) and finally energy-minimized in 500 iterations by steepest descent and 5000 iterations by conjugate gradients. The cutoff for non-bond interactions was always 13 Å except for the two last steps (15 Å). Processing, calculations and analysis were done within

InsightII/Discover version 95.0 (BIOSYM/SI Inc., San Diego).

The electrostatic potential surface was calculated with the program MOLMOL (Koradi *et al*., 1996). The partial charges on all atoms were incorporated. A radius of 1.4 Å was assigned to the solvent (water) and of 2.0 Å to the salt with a concentration of 150 mM. A dielectric constant of 80 for the solvent and of 2 for the molecule was used. The charge cutoff was set at 10 Å.

Acknowledgments

This work was supported by the Belgian National Fund for Scientific Research through a fellowship to F.F. and a NMR equipment grant. This work was supported in part by grant AIR2-CT94-1356 of the Commission of the European Community. The coordinates of the 20 refined conformers and the final constraint list are deposited in the Brookhaven Protein Data Bank under, respectively, PDB identity code 1ayj and r1ayjmr. The scientific responsibility is assumed by the authors.

References

Bloch, C. & Richardson, M. (1991). A new family of small (5 kDa) protein inhibitors of insect (-amylases from seeds of sorghum (*Sorghum bicolor* (L) Moench) have sequence homologies with wheat γ-thionins. *FEBS Letters,* **279**, 101–104.

Bontems, F., Gilquin, B., Roumestand, C., Menez, A. & Toma, F. (1992). Analysis of side chain organization on a refined model of charybdotoxin: structural and functional implications. *Biochemistry,* **31**, 7756–7764.

Broekaert, W. F., Terras, F. R. G., Cammue, B. P. A. & Osborn, R. W. (1995). Plant defensins: novel antimicrobial peptides as components of the host defense system. *Plant Physiol.* **108**, 1353–1358.

Bruix, M., Jiménez, M. A., Santoro, J., González, C., Colilla, F. J., Mendez, E. & Rico, M. (1993). Solution structure of γ1–H and γ1–P thionins from barley and wheat endosperm determined by ^{1}H NMR: a structural motif common to toxic arthropod proteins. *Biochemistry,* **32**, 715–724.

Bruix, M., González, C., Santoro, J., Soriano, F., Rocher, A. & Méndez, E. (1995). ^{1}H-NMR studies on the structure of a new thionin from barley endosperm. *Biopolymers,* **36**, 751–763.

Cociancich, S., Ghazi, A., Hoffmann, J. A. & Letellier, L. (1993). Insert defensin, an inducible antibacterial peptide, forms voltage-dependent channels in *Micrococcus luteus*. *J. Biol. Chem.* **268**, 19239–19245.

Colilla, F., Rocher, A. & Mendez, E. (1990). γ-Purothionins: amino acid sequence of two polypeptides of a new family of thionins from wheat endosperm. *FEBS Letters,* **270**, 191–194.

Cornet, B., Bonmatin, J.-L., Hetru, C., Hoffmann, J. A., Ptak, M. & Vovelle, F. (1995). Refined three-dimensional solution structure of insect defensin A. *Structure,* **3**, 435–448.

Darbon, H., Weber, C. & Braun, W. (1991). Two-dimensional ^{1}H nuclear magnetic resonance study of Aah IT, an anti-insect toxin from the scorpion *Androctonus australis* Hector. Sequential resonance assignments and folding of the polypeptide chain. *Biochemistry,* **30**, 1836–1845.

Dauplais, M., Gilquin, B., Possani, L. D., Gurrola-Briones, G., Roumestand, C. & Ménez, A. (1995). Determination of the three-dimensional solution structure of noxiustoxin: analysis of structural differences with related short-chain scorpion toxins. *Biochemistry,* **34**, 16563–16573.

De Samblanx, G. W., Goderis, I. J., Thevissen, K., Raemaekers, R., Fant, F., Borremans, F. A. M., Acland, D. P., Osborn, R. W., Patel, S. & Broekaert, W. F. (1997). Mutational analysis of a plant defensin from radish (*Raphanus sativus* L.) reveals two adjacent sites important for antifungal activity. *J. Biol. Chem.* **272**, 1171–1179.

Efimov, A. V. (1986). Standard conformations of a polypeptide chain in irregular protein regions. *Mol. Biol. Moscow,* **20**, 250–260.

Efimov, A. V. (1993). Standard structures in proteins. *Prog. Biophys. Mol. Biol.* **60**, 201–239.

Fant, F., Vranken, W. V., Martins, J. C. & Borremans, F. A. M. (1997). Solution structure of *Raphanus sativus* antifungal protein 1 (Rs-AFP1) by ^{1}H Nuclear Magnetic Resonance. Resonance assignments, secondary structure and global fold. *Bull. Soc. Chim. Belg.* **106**, 51–57.

Fernández, I., Romi, R., Szendeffy, S., Martin-Eauclaire, M. F., Rochat, H., Van Rietschoten, J., Pons, M. & Giralt, E. (1994). Kaliotoxin (1–37) shows structural differences with related potassium channel blockers. *Biochemistry,* **33**, 14256–14263.

Fontecilla-Camps, J. C., Habersetzer-Rochat, C. & Rochat, H. (1988). Orthorombic crystals and three-dimensional structure of the potent toxin II from the scorpion *Androctonus australis* Hector. *Proc. Natl Acad. Sci. USA,* **85**, 7443–7447.

Garrill, A., Jackson, S. L., Lew, R. R. & Heath, B. I. (1993). Ion channel activity and tip growth: tip-localized stretch-activated channels generate an essential calcium gradient in the oomycete *Saprolegnia ferx*. *Eur. J. Cell Biol.* **60**, 358.

García, J. R., Arias, F. J., Citores, L., Rojo, M. A., Girbes, T., Bruix, M., Santoro, J., Rico, M., Soriano, F. & Méndez, E. (1993). Estructura tridimensional de una nueva tionina de cebada. In *Proc. SEB,* XVIII Congreso Nacional de Bioquímica, San Sebastian, Spain, Sept. 28.

Griesinger, C., Sørensen, O. W. & Ernst, R. R. (1985). Correlation of connected transitions by 2D NMR spectroscopy. *J. Chem. Phys.* **85**, 6837–6852.

Griesinger, C., Sørensen, O. W. & Ernst, R. R. (1987). Practical aspects of the E. COSY technique. Measurement of the scalar spin-spin coupling constants in peptides. *J. Magn. Reson.* **75**, 474–492.

Güntert, P. & Wüthrich, K. (1991). Improved efficiency of protein structure calculations from NMR data using the program DIANA with redundant dihedral angle constraints. *J. Biomol. NMR,* **1**, 447–456.

Güntert, P., Braun, W., Billeter, M. & Wüthrich, K. (1989). Automated stereospecific ^{1}H NMR assignments and their impact on the precision of protein structure determination in solution. *J. Am. Chem. Soc.* **111**, 3997–4004.

Güntert, P., Braun, W. & Wüthrich, K. (1991). Efficient computation of three-dimensional structures in solution using the program DIANA and the supporting programs CALIBA, HABAS and GLOMSA. *J. Mol. Biol.* **217**, 517–530.

Jablonsky, M. J., Watt, D. D. & Krishna, N. R. (1995). Solution structure of an old world-like neurotoxin

from the venom of the new world scorpion *Centruroides sculpturatus* Ewing. *J. Mol. Biol.* **248**, 449–458.

Jackson, S. L. & Heath, B. I. (1993). Roles of calcium ions in hyphal tip growth. *Microbiol. Rev.* **57**, 367–382.

Johnson, B. A. & Sugg, E. E. (1992). Determination of the three-dimensional structure of iberiotoxin in solution by ^{1}H nuclear magnetic resonance spectroscopy. *Biochemistry,* **31**, 8151–8159.

Johnson, B. A., Stevens, S. P. & Williamson, J. M. (1994). Determination of the three-dimensional structure of Margatoxin by ^{1}H, ^{13}C, ^{15}N triple-resonance nuclear magnetic resonance spectroscopy. *Biochemistry,* **33**, 15061–15070.

Kagan, B. L., Selsted, M. E., Ganz, T. & Lehrer, R. I. (1990). Antimicrobial defensin peptides form voltage-dependent ion-permeable channels in planar lipid bilayer membranes. *Proc. Natl Acad. Sci. USA,* **87**, 210–214.

Kim, Y. & Prestegard, J. H. (1989). Measurement of vicinal couplings from cross peaks in cosy spectra. *J. Magn. Reson.* **84**, 9–13.

Kline, A. D., Braun, W. & Wüthrich, K. (1988). Determination of the complete three-dimensional structure of the α-amylase inhibitor tendamistat in aqueous solution by nuclear magnetic resonance and distance geometry. *J. Mol. Biol.* **204**, 675–724.

Kobayashi, Y., Takashima, H., Tamaoki, H., Kyogoku, Y., Lambert, P., Kuroda, H., Chino, N., Watanabe, T. X., Kimura, T., Sakakibara, S. & Moroder, L. (1991). The cysteine stabilised α-helix: a common structural motif of ion channel blocking neurotoxic peptides. *Biopolymers,* **31**, 1213–1220.

Koradi, R., Billeter, M. & Wüthrich, K. (1996). MOLMOL: a program for display and analysis of macromlecular structures. *J. Mol. Graph.* **14**, 51–55.

Kördel, J., Skelton, N. L., Akke, M. & Chazin, W. J. (1993). High-resolution solution structure of calcium-loaded calbindin D_{9k}. *J. Mol. Biol.* **231**, 711.

Kraulis, P. J. (1991). MOLSCRIPT: a program to produce both detailed and schematic plots of protein structures. *J. Appl. Crystallog.* **24**, 946–950.

Krezel, A. M., Kasibhatla, , Hidalgo, P., MacKinnon, R. & Wagner, G. (1995). Solution structure of the potassium channel inhibitor agitoxin 2: caliper for probing channel geometry. *Protein Sci.* **4**, 1478–1489.

Kumar, A., Wagner, G., Ernst, R. R. & Wüthrich, K. (1980). Studies of *J*-connectivities and selective ^{1}H-^{1}H Overhauser effects in H_2O solutions of biological macromolecules by two-dimensional NMR experiments. *Biochem. Biophys. Res. Commun.* **96**, 1156–1163.

Landon, C., Cornet, B., Bonmatin, J.-M., Kopeyan, C., Rochat, H., Vovelle, F. & Ptak, M. (1996). ^{1}H-NMR-derived structure and the overall fold of the potent anti-mammal and anti-insect toxin III. *Eur. J. Biochem.* **236**, 395–404.

Laskowski, R. A., MacArthur, M. W., Moss, D. S. & Thornton, J. M. (1993). PROCHECK: a program to check the stereochemical quality of protein structures. *J. Appl. Crystallog.* **26**, 283–291.

Lebreton, F., Delepierre, M., Ramírez, A. N., Balderas, C. & Possani, L. D. (1994). Primary and NMR three-dimensional structure determination of a novel crustacean toxin from the venom of the scorpion *Centruroides limpidus limpidus* Karsch. *Biochemistry,* **33**, 11135–11149.

Lee, W., Jablonsky, M. J., Watt, D. D. & Krishna, N. R. (1994). Proton nuclear magnetic resonance and distance geometry/simulated annealing studies on the variant-1 neurotoxin from the new world scorpion *Centruroides sculpturatus* Ewing. *Biochemistry,* **33**, 2468–2475.

Lippens, G., Najib, J., Wodak, S. J. & Tartar, A. (1995). NMR sequential assignments and solution structure of chlorotoxin, a small scorpion toxin that blocks chloride chammels. *Biochemistry,* **34**, 13–21.

Marion, D. & Wüthrich, K. (1983). Application of phase sensitive 2D correlated spectroscopy (COSY) for measurements of ^{1}H-^{1}H spin coupling constants in proteins. *Biochem. Biophys. Res. Commun.* **113**, 967–974.

Mendez, E., Moreno, A., Colilla, F., Pelaez, F., Limas, G. G., Mendéz, R., Soriano, F., Salinas, M. & Haro, C. D. (1990). Primary structure and inhibition of protein synthesis in eukaryotic cell-free system of a novel thionin, γ-hordothionin, from barley endosperm. *Eur. J. Biochem.* **194**, 533–539.

Mikou, A., LaPlante, S. R., Guittet, E., Lallemand, J.-Y., Martin-Eauclaire, M.-F. & Rochat, H. (1992). Toxin III of the scorpion *Androctonus australis* Hector: proton nuclear magnetic resonance assignments and secondary structure. *J. Biomol. NMR,* **2**, 57–70.

Moore, J. M., Lepre, C. A., Gippert, G. P., Chazin, W. J., Case, D. A. & Wright, P. A. (1991). High-resolution structure of reduced French bean plastocyanin and comparison with the crystal structure of poplar plastocyanin. *J. Mol. Biol.* **221**, 533–555.

Nagayama, K. & Wüthrich, K. (1981). Structural interpretation of vicinal ^{1}H-^{1}H coupling constants $^{3}J_{H\alpha H\beta}$ in the basic pancreatic trypsin inhibitor measured by 2D J resolved NMR spectroscopy. *Eur. J. Biochem.* **115**, 653–657.

Neuhaus, D., Wagner, G., Vašák, M., Kägi, J. H. R. & Wüthrich, K. (1985). Systematic application of high-resolution phase-sensitive 2D ^{1}H NMR techniques for the identification of the amino acid proton spin systems in proteins. Rabbit metallothionein-2. *Eur. J. Biochem.* **151**, 257–273.

Nürnberger, T., Nennstiel, D., Jabs, T., Sacks, W. R., Hahlbrock, K. & Scheel, D. (1994). High-affinity binding of a fungal oligopeptide elicitor to parsley plasma membranes triggers multiple defense responses. *Cell,* **78**, 449–460.

Orengo, C. A. & Thornton, J. M. (1993). Alpha plus beta folds revisited: some favoured motifs. *Structure,* **1**, 105–120.

Osborn, R. W., De Samblanx, G. W., Thevissen, K., Goderis, I., Torrekens, S., Van Leuven, F., Attenborough, S., Rees, S. B. & Broekaert, W. F. (1995). Isolation and characterization of plant defensins from seeds of Asteraceae, Hippocastanaceae and Saxifragaceae. *FEBS Letters,* **368**, 257–262.

Rance, M., Sørensen, O. W., Bodenhausen, G., Wagner, G., Ernst, R. R. & Wüthrich, K. (1983). Improved spectral resolution in COSY ^{1}H NMR spectra of proteins via double quantum filtering. *Biochem. Biophys. Res. Commun.* **117**, 479–485.

Richardson, J. S. & Richardson, D. C. (1989). *Prediction of Protein Structure and the Principles of Protein Conformation* (Fasman, G. D., ed.), pp. 1–98, Plenum Press, London.

Schmitt, M. J. & Compain, P. (1995). Killer toxin resistant Kre12 mutants of *Saccharomyces cerevisiae*: genetic and biochemical evidence for a secondary K1 membrane receptor. *Arch. Microbiol.* **164**, 435–443.

Skelton, N. J., Kördel, J. & Chazin, W. J. (1995). Determination of the solution structure of apo calbindin D_{9k} by NMR spectroscopy. *J. Mol. Biol.* **249**, 441–462.

Terras, F. R. G., Schoofs, H. M. E., De Bolle, M. F. F., Van Leuven, F., Rees, S. B., Vanderleyden, J., Cammue, B. P. A. & Broekaert, W. F. (1992). Analysis of two novel classes of antifungal proteins from radish (*Raphanus sativus* L.) seeds. *J. Biol. Chem.* **267**, 15301–15309.

Terras, F. R. G., Torrekens, S., Van Leuven, F., Osborn, R. W., Vanderleyden, J., Cammue, B. P. A. & Broekaert, W. F. (1993). A new family of basic cysteine-rich plant antifungal proteins from Brassicaceae-species. *FEBS Letters,* **316**, 233–240.

Terras, F. R. G., Eggermont, K., Kovaleva, V., Raikhel, N. V., Osborn, R. W., Kester, A., Rees, S. B., Torrekens, S., Van Leuven, F., Vanderleyden, J., Cammue, B. P. A. & Broekaert, W. F. (1995). Small cysteine-rich antifungal proteins from radish: their role in host defence. *Plant Cell,* **7**, 573–588.

Thevissen, K., Ghazi, A., De Samblanx, G. W., Brownlee, C., Osborn, R. W. & Broekaert, W. F. (1996). Fungal membrane responses induced by plant defensins and thionins. *J. Biol. Chem.* **271**, 15018–15025.

Thevissen, K., Osborn, W. O., Acland, D. P. & Broekaert, W. F. (1997). Specific, high affinity binding sites for an antifungal plant defensin on *Neurospora crassa* hyphae and microsomal membranes. *J. Biol. Chem.* **272**, 32176–32181.

Weiner, S. J., Kollman, P. A., Case, D. A., Singh, C., Ghio, C., Alagona, G., Profeta, S. & Weiner, P. (1984). A new force field for molecular mechanical simulation of nucleic acids and proteins. *J. Am. Chem. Soc.* **106**, 765–784.

Wider, G., Hosur, R. V. & Wüthrich, K. (1983). Suppression of the solvent resonance in 2D NMR spectra of proteins in H_2O solution. *J. Magn. Reson.* **52**, 130–135.

Widmer, H., Billeter, M. & Wüthrich, K. (1989). Three-dimensional structure of the neurotoxin ATX Iα form *Anemonia sulcata* in aqueous solution determined by nuclear magnetic resonance spectroscopy. *Proteins: Struct. Funct. Genet.* **6**, 357–377.

Widmer, H., Widmer, A. & Braun, W. (1993). Extensive distance geometry calculations with different NOE calibrations: new criteria for structure selection applied to Sandostatin and BPTI. *J. Biomol. NMR,* **3**, 307–324.

Williamson, M. P., Havel, T. F. & Wüthrich, K. (1985). Solution conformation of proteinase inhibitor IIA from bull seminal plasma by ^{1}H NMR and distance geometry. *J. Mol. Biol.* **182**, 295–315.

Yao, J., Dyson, H. J. & Wright, P. E. (1994). 3D structure of a type VI turn in a linear peptide in water solution. *J. Mol. Biol.* **243**, 754–766.

Zhao, B., Carson, M., Ealick, S. E. & Bugg, C. E. (1992). Structure of scorpion toxin variant-3 at 1.2 Å resolution. *J. Mol. Biol.* **227**, 239–252.

Zimmerman, S., Nürnberger, T., Frachisse, J. H., Wirtz, W., Guern, J., Hedrich, R. & Scheel, D. (1997). Receptor mediated activation of a plant Ca^{2+} permeable ion channel involved in pathogen defense. *Proc. Natl Acad. Sci. USA,* **94**, 2751–2755.

Zuiderweg, E. R. P., Boelens, R. & Kaptein, R. (1985). Stereospecific assignments of ^{1}H NMR methyl lines and conformation of valyl residues in the lac repressor headpiece. *Biopolymers,* **24**, 601–611.

Edited by P. E. Wright

(Received 10 November 1997; received in revised form 3 March 1998; accepted 4 March 1998)